Super-resolution imaging through a planar silver layer

David O. S. Melville and Richard J. Blaikie

MacDiarmid Institute for Advanced Materials and Nanotechnology, Department of Electrical and Computer Engineering, University of Canterbury, Christchurch, NEW ZEALAND
dom15@student.canterbury.ac.nz, r.blaikie@elec.canterbury.ac.nz

Abstract: It has been proposed that a planar silver layer could be used to project a super-resolution image in the near field when illuminated near its plasma frequency [J. B. Pendry, Phys. Rev. Lett. **86**, 3966 (2000)]. This has been investigated experimentally using a modified form of conformal-mask photolithography, where dielectric spacers and silver layers are coated onto a tungsten-on-glass mask. We report here on the experimental confirmation that super-resolution imaging can be achieved using a 50-nm thick planar silver layer as a near-field lens at wavelengths around 365 nm. Gratings with periods down to 145 nm have been resolved, which agrees well with our finite-difference time domain (FDTD) simulations.

OCIS codes: (100.6640 Superresolution; (110.5220) Photolithography; (260.3910) Metals, optics of; (240.6680) Surface plasmons.

References and links

1. J. B. Pendry, "Negative refraction makes a perfect lens," Phys. Rev. Lett. **85**, 3966–3969 (2000).
2. R. A. Shelby, D. R. Smith and S. Schultz, "Experimental verification of a negative index of refraction," Science **292,** 77–79 (2001).
3. A. N. Lagarkov and V. N. Kissel, "Near-perfect imaging in a focusing system based on a left-handed-material plate," Phys. Rev. Lett. **92,** art. no. 077401 (2004).
4. D. O. S. Melville, R. J. Blaikie and C. R. Wolf, "Submicron imaging with a planar silver lens," Appl. Phys. Lett. **84**, 4403–4405 (2004).
5. R. J. Blaikie and D. O. S. Melville, "Imaging through planar silver lenses in the optical near field," J. Opt. A: Pure Appl. Opt. **7**, S176–S183 (2005).
6. M. M. Alkaisi, R. J. Blaikie, S. J. McNab, R. Cheung and D. R. S. Cumming, "Sub-diffraction-limited patterning using evanescent near-field optical lithography," Appl. Phys. Lett. **75**, 3560–3562 (1999).
7. X. G. Luo and T. Ishihara, "Subwavelength photolithography based on surface-plasmon polariton resonance," Opt. Express **12**, 3055–3065 (2004), http://www.opticsexpress.org/abstract.cfm?URI=OPEX-12-14-3055.
8. H. F. Talbot, "Facts relating to optical science," Phil. Mag. **9**, 401–407 (1836).

1. Introduction

The near-field imaging properties of plasmonic systems have attracted a great deal of interest since Pendry's proposal [1] that a metal film illuminated near its plasma frequency could be used for super-resolution imaging. Super-resolution is defined here as resolution beyond the conventional diffraction limit for far-field imaging. For normal-incidence illumination at wavelength λ the smallest spatial frequency that can be resolved in a far-field image is λ/n, where n is the refractive index of the surrounding medium.

Pendry's proposal, together with his predictions for the properties of negative-refractive-index (NRI) materials, has sparked a great deal of interest from the optics and electromagnetics community. There have now been microwave-frequency demonstrations of negative refraction [2] and sub-wavelength imaging [3] with metamaterials, and we report here on the experimental confirmation that super-resolution imaging can be achieved at

#6547 - $15.00 US Received 2 February 2005; revised 7 March 2005; accepted 12 March 2005

optical wavelengths. A 50-nm thick planar silver layer has been used as a near-field lens at wavelengths around 365 nm, for imaging a tungsten-on-glass mask into nearby photoresist.

Near-field imaging through silver has recently been reported with sub-micron [4] and sub-wavelength [5] resolution; however the silver layers used in these studies were too thick to allow significant enhancements of evanescent field components, hence super-resolution was not achieved (nor was it expected). By carefully refining our experimental procedures we can now form planar silver lens structures that are sufficiently thin (50 nm) and flat (~1nm root-mean-square (rms) roughness) to show unambiguous super-resolution imaging. The experimental details are outlined in the following section and the key results are presented in Section 3. Finite-difference time domain simulations of the imaging process have also been carried out, and the results of these are presented in Section 4, before the concluding remarks and acknowledgements are given.

2. Experimental methods

The experimental methods we have used are based on previous near-field imaging work [4–6], in which a conformable tungsten-on-glass mask is used to ensure intimate contact with the photoresist that is used to capture the near-field image. The experimental setup is shown schematically in Fig 1. Tungsten masks are patterned onto a conformable glass substrate using electron-beam lithography (EBL), followed by the deposition of additional dielectric spacer and silver lens layers. The finished masks are then brought into vacuum contact with a resist stack for lithographic exposures. A detailed explanation of the processes can be found in Refs. 4 and 5, but the key improvements to the process that have enabled super-resolution imaging to be achieved are given below.

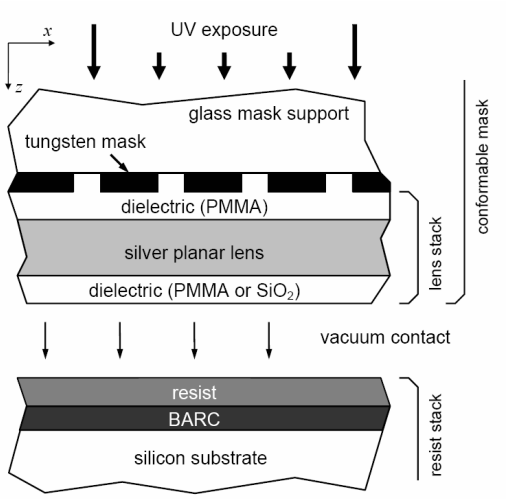

Fig. 1. Schematic diagram of the near-field imaging experimental arrangement. A bottom anti-reflection coating (BARC) layer is used beneath the resist to prevent substrate reflections.

The tungsten-on-glass masks are built on 200-μm thick, 25-mm diameter glass coverslips. These are metalised with a 30-nm thick tungsten film and patterned using EBL and reactive ion etching (RIE); patterns include isolated lines, line pairs, gratings and arrays of dots, with feature sizes from 5 μm to less than 100 nm.

Additional dielectric spacer and silver lens layers are then deposited to form the 'lens stack' arrangement shown in Fig. 1. The first dielectric layer has two functions: providing a means of spacing the silver from the mask, and planarising the tungsten mask to smooth out the uneven topology before the silver lens layer is deposited. This planarisation is critical to the experiment, as if there is significant topography transferred through to the silver then any images that result may be caused by this instead of the desired planar lensing property; the

#6547 - $15.00 US Received 2 February 2005; revised 7 March 2005; accepted 12 March 2005

ability of topographic features on silver to cause sub-wavelength patterning of photoresist has been studied in its own right [7], which we wish to avoid for these experiments.

To achieve a planar first dielectric spacer a layer of poly-methylmethacrylate (PMMA) is spun on to about 5 times the thickness required, before being re-flowed overnight at 185 ºC to increase planarisation and then dry-etched back to give the necessary thickness. An oxygen RIE process is used to etch back the spacer (40 sccm O_2, 100 W, 100 mTorr). It was determined that a lower power and high gas flow rate etch produced the smoothest surface, with typical values for the roughness of the final PMMA surface being less than 0.8 nm rms.

The next step is to deposit the silver film onto the stack. Both thermal evaporation and DC magnetron sputtering were used for deposition, with the main goal being to produce the smoothest silver layer possible. Deposition rates of 0.5 nm/s and 1.4 nm/s were used for sputtering or evaporation respectively, and in both cases the resultant films had surface roughness values of less than 1.2 nm rms (approx 10 nm peak-peak).

In our earlier work the final spacer layer was PMMA [4], but SiO_2 has been found to give more consistent and robust results. The way in which the SiO_2 is deposited is dependent on the silver deposition; the same method is used for both layers so that the SiO_2 can be deposited without the need to break vacuum, which minimizes oxidation and sulfidation of the silver. An AFM image of the surface of this final spacer layer is shown in Fig. 2 for a mask with a 25-nm thick PMMA spacer, a 50-nm thick evaporated silver lens and a 10-nm thick evaporated SiO_2 spacer (we will refer to this as a 25/50/10-PMMA/Ag/SiO_2 mask). The image is taken on top of a region with a 350-nm period grating in the 30-nm thick tungsten layer, and none of this topography has been transferred through the subsequent layers. The surface roughness of the final mask is approximately 1.2 nm rms, the same as for the silver layer underneath.

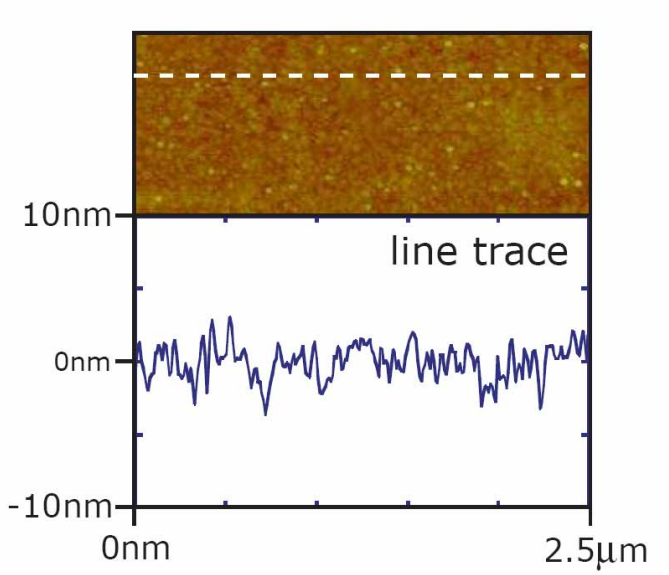

Fig. 2. AFM image and line trace taken on the surface of the SiO_2 layer of a 25/50/10-PMMA/Ag/SiO_2 lens stack, directly above a 350-nm period grating in the underlying tungsten.

Exposures are performed by mounting the masks onto a rigid support that is compatible with a commercial optical mask aligner (Karl Süss MA-6). The mask aligner is used in soft-vacuum contact mode with an unfiltered 350 W mercury lamp light source, which gives an intensity of 6.7 mW/cm^2 at the centre of the exposure field. Unfiltered exposure was used to ensure that the plasmonic resonance condition for superlensing was met somewhere across the lamp's pressure-broadened i-line emission that is centered at 365 nm. Wavelengths that do not meet this resonance condition will be self-filtered by the silver layer.

#6547 - $15.00 US Received 2 February 2005; revised 7 March 2005; accepted 12 March 2005

The substrates used for the exposures are from either a prime grade p-type four-inch silicon wafer that is cut into 25-mm square samples, or directly from one-inch silicon wafers. The one-inch wafers have been found to give better results, as intimate contact is achieved more reliably; cleaving dust often remains on the diced 25-mm square samples, which can prevent intimate contact over the surrounding areas.

The samples are ultra-sonically cleaned in acetone, methanol, and IPA before applying bottom anti-reflection coating (BARC) and imaging photoresist layers. The BARC (Clariant BARLi-II-200) is spun on to a thickness of approximately 200 nm, and the photoresist (Clariant HiR1075 diluted 1:4 with methyl amyl ketone) is spun on at 4000 rpm for 60 s, giving a thickness of 120 nm. This is somewhat thicker than other resist we have used in the past (typically 50-nm thick), but super-resolution imaging is achieved nonetheless.

Exposure times were established by observing results from multiple exposures, and ranged from 4 to 120 s. An AZ300MIF developer (aqueous 2.38% tetra-methyl ammonium hydroxide) was used, and development times ranged from 2 to 8 s. Shallow exposures required that the resulting patterns be imaged using an atomic force microscope (AFM) from Digital Instruments (model Dimension 3100).

3. Experimental results

An example imaging result is shown in Fig. 3, for a 1-μm period grating exposed for 120 s through the 25/50/10-PMMA/Ag/SiO_2 mask and developed for 3 s. The image fidelity is much improved over earlier results for a 60/120/60-PMMA/Ag/PMMA lens stack [4], and the line scan across this image shown in Fig. 3(b) shows that the image is fully developed into the 120-nm thick resist. Imaging of sub-micron features has therefore been greatly improved by using thinner silver and spacer layers, and by reducing the surface roughness of the lens stack.

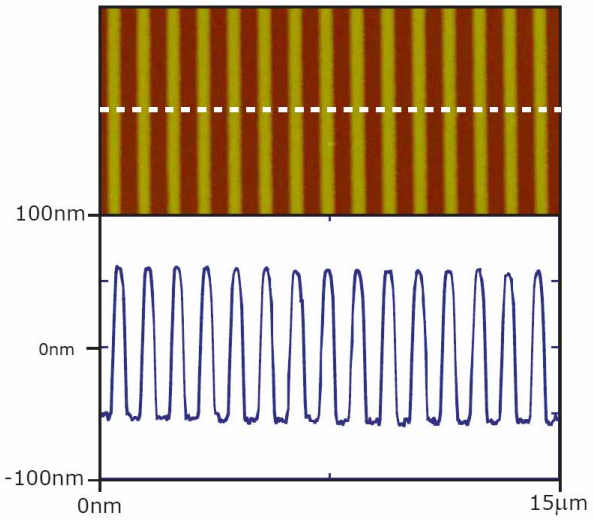

Fig. 3. AFM image and line scan of a 1-μm period grating exposed through the 25/50/10-PMMA/Ag/SiO_2 lens stack. The height scale on the AFM image is 130 nm.

The ability of the silver lenses to image gratings has been used as the ultimate resolution test, as there is a hard limit for the ability of a conventional (far field) lens to image a periodic object (diffraction grating). For normal-incidence illumination the minimum spatial period that can be resolved with wavelength λ through a medium with refractive index n is

$$p_{\min} = \lambda / n \ , \qquad (1)$$

which corresponds to the period below which only a zeroth order diffracted beam will propagate beyond the grating. Zero contrast would therefore be expected in any far-field image below this limit, no matter how good the imaging resist might be. For our exposures at

#6547 - $15.00 US Received 2 February 2005; revised 7 March 2005; accepted 12 March 2005

365 nm wavelength and with $n = 1.5$ for the refractive index of the final SiO_2 spacer layer Eq. (1) gives a diffraction-limited resolution of $p_{min} = 243$ nm.

Figure 4 shows a series of grating images, exposed through the 25/50/10-PMMA/Ag/SiO_2 lens stack under the same conditions as for the 1-μm period grating shown in Fig. 3. Gratings with periods from 500 nm down to 170 nm are resolved, with the depth of the modulation in the resist reducing as the grating period reduces. All of the gratings with periods above the diffraction limit (243 nm) are well resolved (Fig. 4(a) to (d)), and similar results have been reported earlier for thicker silver lenses (although not with resolution down to 250-nm period). We note that even though this resolution is not sub-diffraction-limited, the silver lens is still having a beneficial effect in reconstructing the image, as such high resolution is not expected in proximity exposures through dielectric spacers of the same thickness as this lens stack [5].

The key results of this work are those shown in Figs. 4(e) and (f), which are for sub-diffraction-limited gratings (200 nm and 170 nm periods respectively). In both cases the gratings are resolved, indicating that the effect is not due to classical reduction self-imaging (the Talbot effect [8]). The contrast has degraded in these images compared to the gratings with periods greater than 250 nm, but the fact that they are present at all gives experimental confirmation of Pendry's controversial superlensing proposal [1].

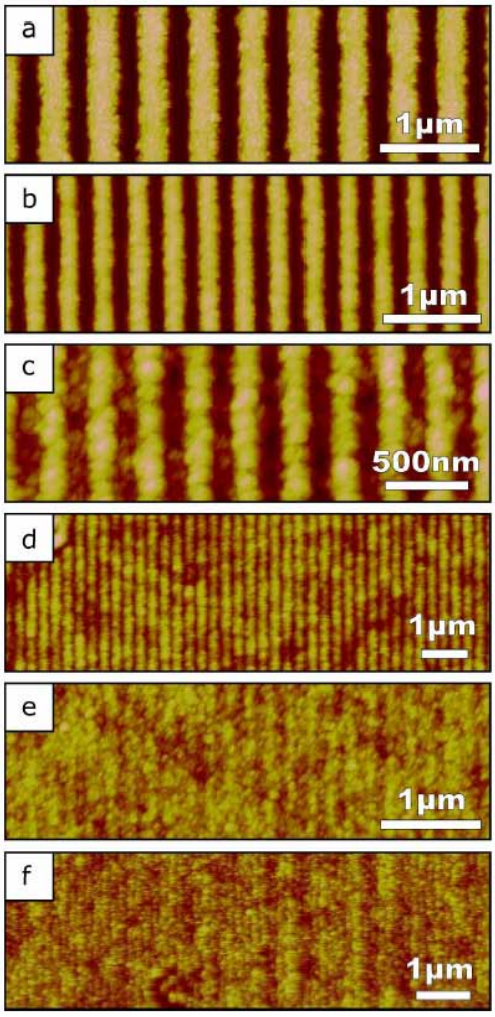

Fig. 4. AFM images of gratings imaged through the 25/50/10-PMMA/Ag/SiO_2 lens stack, with periods of (a) 500 nm, (b) 350 nm, (c) 290 nm, (d) 250 nm, (e) 200 nm and (f) 170 nm.

#6547 - $15.00 US Received 2 February 2005; revised 7 March 2005; accepted 12 March 2005

Gratings with periods down to 145 nm have also been resolved in this exposure, as shown in Fig. 5. In this case the grating is weaker than the background roughness of the developed photoresist, so a Fourier transform of the image is required to confirm that the grating has been resolved; this is shown in Fig. 5(b) for the direction parallel to the grating vector $\boldsymbol{k}_g$. Similar analyses of the images of 120-nm period gratings do not reveal any features in the spatial Fourier transform at 120 nm period, so the resolution of this lens for the exposure and development conditions used lies between 120 and 145 nm period.

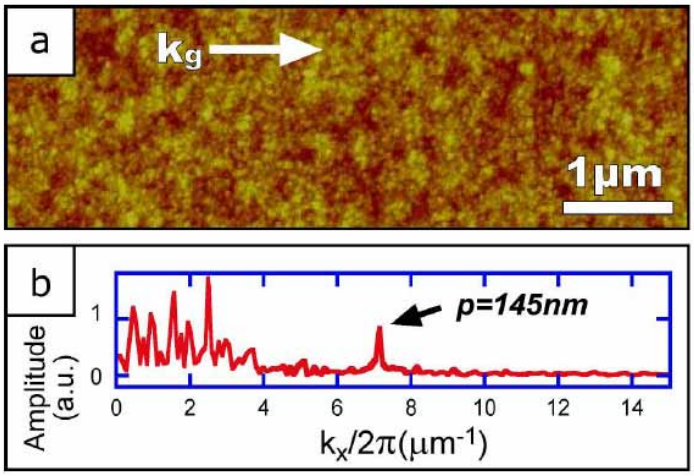

Fig. 5. Results for a 145-nm period grating exposed through the 25/50/10-PMMA/Ag/SiO_2 lens stack: (a) AFM image and (b) Fourier transform in the direction of the grating vector $\boldsymbol{k}_g$.

4. FDTD simulations

Finite-difference time domain (FDTD) electromagnetic simulations have been used in conjunction with the experimental studies, in order to determine the intensity profiles that are expected in the resist, and the ultimate resolution that can be expected. The details of the simulation techniques that we have employed have been described previously [5]; we have performed simulations for the six dominant lines of the mercury lamp between 312 nm and 436 nm, and can provide weighted superpositions of these if we wish. We present here results for single-frequency exposure at a wavelength of 365 nm.

Line traces of the intensity profile 25 nm below the surface of the photoresist are shown in Fig. 6 for two gratings exposed through a 25/50/10-PMMA/Ag/SiO_2 lens stack, with periods of 300 nm (above the diffraction limit) and 200 nm (below the diffraction limit). The intensity modulation in the image is weaker for the sub-diffraction limited case, which agrees qualitatively with our experimental observations (Fig. 4). From such line traces we can determine the maximum and minimum intensity in a simulated image, I_{max} and I_{min} respectively, and use these to calculate the image contrast

$$V = \frac{I_{max} - I_{min}}{I_{max} + I_{min}} , \qquad (2)$$

from which the resolution of the imaging process can be determined.

#6547 - $15.00 US Received 2 February 2005; revised 7 March 2005; accepted 12 March 2005

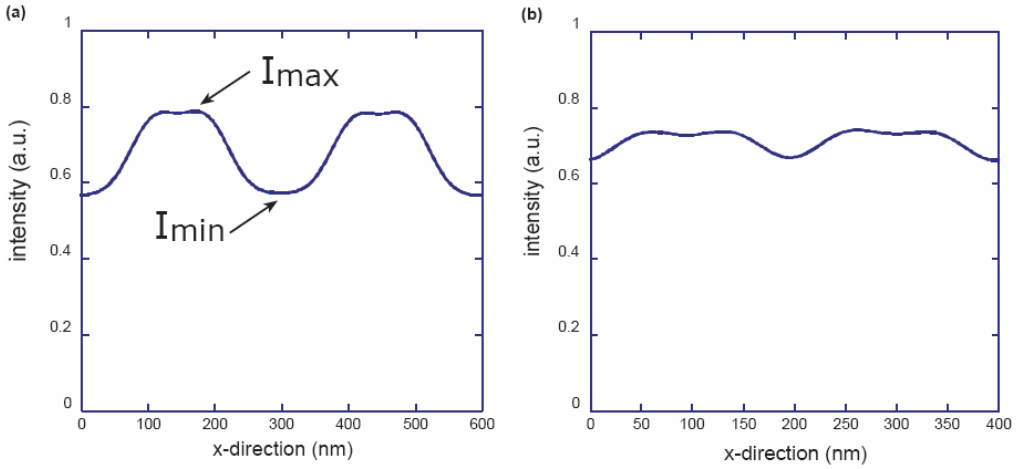

Fig. 6. Simulated intensity profiles 25 nm below the photoresist surface for exposure through the 25/50/10-PMMA/Ag/SiO_2 lens stack. Grating periods are (a) 300 nm and (b) 200 nm.

The image contrast has been extracted from the simulations for a wide range of grating periods, from 800 nm all the way down to 40 nm, and the results are shown in Fig. 7. There is a reduction in image contrast for grating periods from 800 nm down to 190 nm, and then a recovery from 190 to 100 nm. There is some evidence of this effect in our experiments, as the 170-nm period grating is actually slightly better resolved than the 200-nm period one. However, this is still a rather subjective conclusion to draw, as other factors such as the duty cycle in the experimental gratings could be influencing the experimental results.

For periods below 120 nm the simulated image contrast drops rapidly, although there is still a small amount of contrast remaining ($V < 0.01$) even for 40-nm period gratings, which is about $1/6^{th}$ of the diffraction-limited resolution. We note that the image contrast would be zero for all gratings below 243 nm period for the equivalent far-field images.

The simulation results give a more optimistic estimate of the image resolution (sub-100 nm) than we have obtained experimentally (120–145 nm), which is not too surprising. This indicates that if we are able to further reduce the surface roughness of our films we may be able to attain images at or below 100-nm period. In order to obtain higher resolution still the thickness of the silver and spacer layers can be reduced further, or losses can be reduced to give better enhancements of evanescent fields. The first case can be explored experimentally, although there will be a point at which the silver and spacer layers are so thin that hard-contact evanescent-field exposure would be preferable. Engineering the losses in the silver layer will also be difficult, as these are largely determined by the nature of the material itself; silver has the lowest loss of common plasmonic materials at visible and ultraviolet wavelengths.

#6547 - $15.00 US Received 2 February 2005; revised 7 March 2005; accepted 12 March 2005

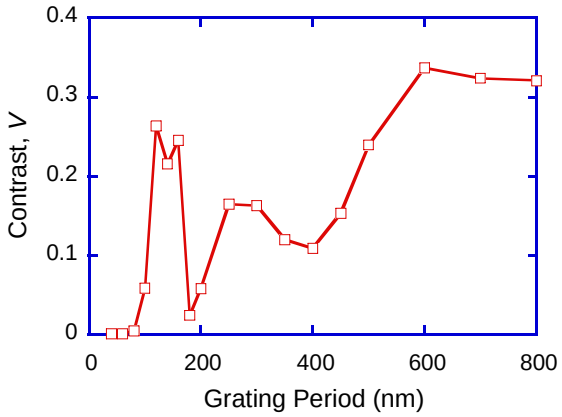

Fig. 7. Simulated image contrast *V* as a function of grating period, extracted 25-nm below the surface of the resist for exposure through a 25/50/10-PMMA/Ag/SiO_2 lens stack.

5. Conclusions

Super-resolution imaging through a planar silver layer has been obtained experimentally by using a modified conformal-mask photolithography experiment. This confirms a controversial prediction, and completes the set of experimental verifications of phenomena related to negative-refractive-index materials that were made in Ref [1].

A 50-nm thick silver layer has been used as the near-field lens, together with a total of 35 nm of additional dielectric spacers. By controlling the planarity of the lens and spacer layers, and by reducing the surface roughness to approximately 1 nm rms images of gratings with periods down to 145 nm have been resolved. For grating periods larger than this the image contrast increases with increasing period, indicating that the results are not caused by any period-reduced self imaging process (Talbot effect), which would only give images of selected gratings (those that matched a Talbot distance criterion) for a fixed mask-resist separation.

Full electromagnetic simulations have also been carried out, and these are in general agreement with our experimental findings. A marked reduction in image contrast is predicted around the diffraction limit, but some contrast persists all the way down to sub-100 nm period gratings. This work has shown that it is possible to relax the usual near field criterion that resolution degrades rapidly away from an aperture (or an arbitrary object), giving back to optical scientists and engineers a 'working distance' degree of freedom for designing super-resolution near field optical systems.

Acknowledgments

The authors wish to thank Dr Maan Alkaisi, Conrad Wolf, Alan Wright and Andrew Thomson for collaboration and laboratory assistance, and Helen Devereux and Gary Turner for technical support. Useful discussions with Hank Smith and James Goodberlet (MIT) are also acknowledged. This research was supported financially by the Marsden Fund of the Royal Society of New Zealand (contract UOC-312). David also acknowledges the financial support of the University of Canterbury Brownlie Scholarship, and Richard acknowledges support from Fulbright New Zealand during the early stages of this work.